Journal of Solid State Chemistry **147,** 624–630 (1999)
Article ID jssc.1999.8426, available online at http://www.idealibrary.com on IDEAL®

Cristobalite-Related Phases in the $KAlO_2$–$KAlSiO_4$ System

Shamus L. G. Husheer, John G. Thompson, and Alexandra Melnitchenko

Research School of Chemistry, Australian National University, Canberra, ACT 0200, Australia

Received March 29, 1999; in revised form June 4, 1999; accepted June 8, 1999

A study of the K-rich end of the potassium aluminate–silica system ($K_{1-x}Al_{1-x}Si_xO_2$; $0 \le x \le 0.25$) at temperatures up to 1500°C has confirmed the existence of a cubic cristobalite-type solid solution extending to $x \approx 0.235$ at 1500°C. The end member, $KAlO_2$, transforms on cooling to an orthorhombic $KGaO_2$-type structure at 531°C (orthorhombic *Pbca*: $a = 5.4327(8)$, $b = 10.924(2)$, $c = 15.469(2)$ Å, $Z = 16$). The room temperature structure has been modeled using chemically restrained refinement of Guinier-Hägg X-ray powder diffraction (XRD) data by the Rietveld method (reduced $\chi^2 = 0.074$, wRp = 0.065, Rp = 0.049). With progressive substitution of SiO_2 into $KAlO_2$ the cubic-to-orthorhombic phase transition temperature is lowered. A new cristobalite-related phase field has been identified as existing close to room temperature between $x \approx 0.10$ and 0.125. The XRD data for this phase can be indexed to a tetragonal superstructure with $a_r = 2\sqrt{2}a_p$ and $c_r = 2c_p$ (r = resultant, p = parent). Analysis of K-rich specimens by XRD and differential scanning calorimetry required extreme care to avoid rapid degradation by atmospheric moisture. © 1999 Academic Press

Key Words: **potassium aluminate; potassium aluminosilicate; cristobalite-type; $KGaO_2$-type; synthesis; Rietveld refinement; cristobalite-related superstructure,; solid solution, XRD.**

INTRODUCTION

The ternary system K_2O–Al_2O_3–SiO_2 has been carefully investigated over many decades because of its fundamental importance to mineralogy and silicate ceramics. The equilibrium phase fields in the pseudobinary $KAlSiO_4$–SiO_2 as a function of temperature and pressure were established in the period from the 1920s to the late 1950s and are summarized in Fig. 407 of Ref. (1). While there were several attempts to synthesize a compound of stoichiometry, $K_2Al_2SiO_6$ (2, 3), it was only more recently that phase relationships in the $KAlO_2$–$KAlSiO_4$ pseudobinary were systematically worked out.

Li *et al.* (4) concentrated on the K-rich end of the $KAlO_2$–$KAlSiO_4$ pseudobinary and reported a maximum solubility of SiO_2 in $KAlO_2$ of 20 mol% at 900°C. Cook *et al.* (5) proposed a tentative equilibrium phase diagram for the $KAlO_2$–$KAlSiO_4$ join as a function of temperature. More detail was subsequently added by these authors and reported in a later review paper (6).

In the present study our focus is on the cristobalite-related solid solution $K_{1-x}Al_{1-x}Si_xO_2$ ($0 \le x \le 0.22$) at 1500°C (6) at the K-rich end of the $KAlO_2$–$KAlSiO_4$ pseudobinary. In a recent transmission electron microscopy (TEM) and X-ray powder diffraction (XRD) study of the analogous $NaAlO_2$–$NaAlSiO_4$ pseudobinary at about 1200°C (7) we identified five new cristobalite-related phases at intermediate compositions in what was previously thought to be a continuous solid solution. On this basis we considered that closer investigation of the cristobalite-related solid solution in the K-containing system was justified.

$KAlO_2$, the end member of the subject "cubic" solid solution between $0 \le x \le 0.22$ in the system $K_{1-x}Al_{1-x}Si_xO_2$, has been studied in its own right. XRD data were first reported for material synthesized at 1650°C by Brownmiller (8), and Barth (9) identified cubic $KAlO_2$ as being cristobalite-related. Two more recent thermodynamic studies (10, 11) identified a reversible phase transition for $KAlO_2$ at 522–535°C with the higher temperature form having cubic symmetry and being unquenchable and the lower temperature form having lowered symmetry. Otsubo *et al.* (10) also reported the *d*-spacing for the 220 reflection as a function of temperature up to 1050°C.

In a study of $KFeO_2$, Pistorius and de Vries (12) stated that "$KAlO_2$ probably has the same structure" as $KGaO_2$, but this comment does not appear to be based on any experimental evidence. While other authors have accepted that the room-temperature form of $KAlO_2$ has a cristobalite-related structure with symmetry lower than cubic, XRD data for the lower symmetry phase, other than those of Brownmiller (8) from 1935, and determination of the unit cell or space group symmetry appear not to have been reported.

Consequently the aims of this study are

(i) to reinvestigate the cristobalite-related solid solution at the K-rich end of the $KAlO_2$–$KAlSiO_4$ pseudobinary to look for new cristobalite-related phases as observed in the $NaAlO_2$–$NaAlSiO_4$ pseudobinary,

0022-4596/99 $30.00

(ii) to determine the unit cell, space group symmetry, and crystal structure of the end member $KAlO_2$ at room temperature, and

(iii) to define the phase field for the low temperature structure as a function of temperature and composition.

SYNTHESIS

$K_{1-x}Al_{1-x}Si_xO_2$ Specimens with $x > 0$

Potassium aluminosilicate specimens were synthesized from colloidal silica containing 32 wt% SiO_2 (Ludox AM, du Pont), potassium nitrate (AnalaR, BDH), and aluminium nitrate nonahydrate (AnalaR, BDH) for compositions $x = 0.025, 0.05, 0.075, 0.1, 0.125, 0.15, 0.175, 0.2$, and 0.25. In each case specimens were prepared by mixing KNO_3 and $Al(NO_3)_3 \cdot 9H_2O$ in a 1:1 mole ratio, dissolving the mixture in a minimum quantity of warm (30–35°C) distilled water, and then adding the stoichiometrically required quantity of colloidal silica with stirring while maintaining the temperature between 30 and 35°C. The solutions were dehydrated in an oven at 110°C overnight. The resultant solids were transferred to platinum crucibles and then progressively heated to higher temperatures to remove water and decompose the nitrate. Samples were heated sequentially at 100, 150, 200, 250, 350, 500, and 700°C, typically for several hours or overnight. After each heating the samples were rapidly cooled to room temperature and then remixed in a mortar and pestle. One gram of each sample was pressed into a pellet for final overnight annealing of the samples at 900°C. Cook *et al.* (5) noted that above about 1000°C it was necessary to perform reactions in sealed vessels to prevent volatilization of K_2O.

For each of $x = 0.1$, 0.2, and 0.25 three portions of each (~ 50 mg) were sealed in separate 4 mm in o.d. Pt tubes and fired at 1500°C: One was annealed overnight at this temperature and then quenched in water; a second was cooled to 1200°C, held at this temperature for 16 h, and then quenched in water; and a third was slowly cooled over 4 days from 1500°C to room temperature. As for Cook *et al.* (5) failure of the Pt tube during firing for quenched specimens was indicated by absorption of water.

For each of $x = 0.025, 0.05, 0.075, 0.125, 0.15$, and 0.175 small portions of each were sealed in Pt tubes as above, annealed at 1500°C for 16 h, and then quenched in water.

$KAlO_2$ End Member

$KAlO_2$ was prepared by three methods:

(1) decomposition of nitrates, as described above,

(2) solid state reaction of $K_2CO_3 \cdot 1.5H_2O$ and reactive Al_2O_3, the method used by Cook *et al.* (5), and

(3) dehydration of $K_2Al_2O_4 \cdot 3H_2O$.

In the first method a stoichiometric mixture of KNO_3 and $Al(NO_3)_3 \cdot 9H_2O$ was ground in a mortar and pestle and decomposed in a furnace with temperature ramped to around 350°C over a 2-h period. The sample, now a low-density crystalline solid, was ground to a fine powder and then ramped to 850°C over 3 h. The sample was then reground and annealed at 900°C overnight.

In the second method reactive alumina, produced by decomposing $Al(NO_3)_3 \cdot 9H_2O$ at 350°C overnight, was mixed with a stoichiometric amount of $K_2CO_3 \cdot 1.5H_2O$, fired at 350°C, and then ramped to 850°C over 2 h. The sample was reground and annealed at 900°C overnight.

The third method required the synthesis of well-crystallized potassium aluminate hydrate ($K_2Al_2O_4 \cdot 3H_2O$), which was prepared according to the method of Allen and Rogers (13), under an argon atmosphere and using dry ethanol and then diethyl ether to wash the product. The $K_2Al_2O_4 \cdot 3H_2O$ reagent was stored under argon to prevent reaction with atmospheric CO_2 and H_2O. Confirmation of pure $K_2Al_2O_4 \cdot 3H_2O$ was obtained by XRD and chemical analysis, both of which were consistent with the results of Johansson (14). Dehydration of $K_2Al_2O_4 \cdot 3H_2O$ to generate $KAlO_2$ was performed by ramping to 900°C over a period of 6 h with a final annealing at 900°C overnight.

Samples prepared by each of these methods were sealed in Pt tubes, fired at 1500°C overnight, and then quenched in water. Again, failure of a tube was indicated by absorption of water upon quenching.

To test whether cristobalite-related potassium aluminate was truly a stoichiometric single phase, specimens were prepared according to the nitrate synthesis described above with $\pm 10\%$ potassium relative to the formula $KAlO_2$.

CHARACTERIZATION AND DATA COLLECTION

Specimens were examined after each firing by X-ray powder diffraction (XRD) using a Siemens D5000 diffractometer with Cu$K\alpha$ radiation ($\lambda = 1.5418$ Å) or using a Guinier-Hägg camera with monochromated Cu$K\alpha_1$ radiation ($\lambda = 1.5406$ Å) with Si (NBS No. 640) as an internal standard. Unit cell dimensions of equilibrium specimens were obtained from Guinier-Hägg data. As the $KAlO_2$ and $KAlO_2$-rich specimens were extremely hygroscopic it was necessary to open the sealed Pt tubes under argon or dry nitrogen in a glove box, seal the Guinier-Hägg specimen between two pieces of support tape, and record the film with the camera purged by dry nitrogen. In the air $KAlO_2$ and $KAlO_2$-rich specimens decomposed within tens of seconds of exposure to atmospheric moisture.

The XRD profile of room-temperature $KAlO_2$ used for Rietveld refinement was obtained by scanning a Guinier-Hägg film of the material without Si standard. The resultant step size was $\sim 0.018°$ 2θ and the extracted profile between 19° and 72° 2θ, spanning 309 reflections, was used.

Differential scanning calorimetry (DSC) data were recorded for specimens from $x = 0.0$ to 0.2 using a TA

Instruments 2100 differential scanning calorimeter. Specimens were transferred from freshly opened Pt tubes to Al DSC pans and sealed under dry nitrogen in a glove box. Heating and cooling rates of 20°C per minute were used and the furnace chamber was purged with dry nitrogen.

RESULTS AND DISCUSSION

X-Ray Powder Diffraction

All specimens quenched from 1500°C to room temperature produced sharp Guinier-Hägg films. The specimen at $x = 0.25$ contained a two-phase mixture of the cubic$_{ss}$ end member and the tetragonal phase at $x \approx 0.42$ reported by Cook *et al.* (5). Specimens between $x = 0.2$ and 0.15 comprised the cubic$_{ss}$ phase and could be indexed to the cubic$_{ss}$ $Fd\bar{3}m$ (15) unit cell. Specimens between $x = 0.125$ and 0.10 comprised a single phase similar to the cubic$_{ss}$ phase but with at least five additional lines. Specimens between $x = 0.0$ and 0.05 comprised a single orthorhombic phase, i.e., the low-temperature form of $KAlO_2$ and its solid solution. The specimen at $x = 0.075$ appeared to consist of the two phases on either side in equilibrium. Figure 1 shows representative XRD profiles for the three different phases between 25° and 46.5° 2θ juxtaposed.

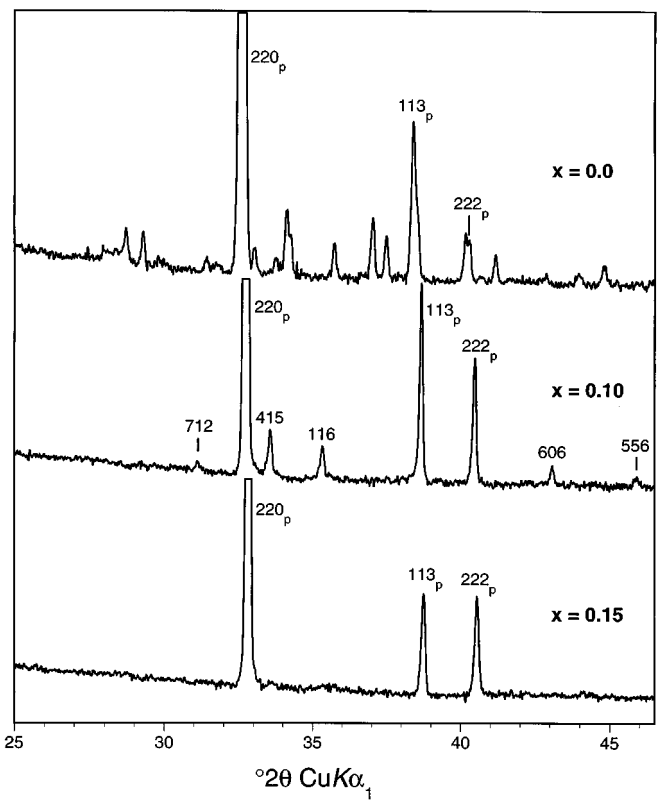

FIG. 1. X-ray powder diffraction profiles between 25 and 46.5° 2θ for $x = 0.0$, $x = 0.10$, and $x = 0.25$ in the system $K_{1-x}Al_{1-x}Si_xO_2$ with truncation of the $\{220\}_p^*$ (p = parent) reflections at $\sim 32.8°$ 2θ. The satellite reflections in the $x = 0.10$ profile are indexed according to the resultant unit cell. The three profiles $x = 0.0$, $x = 0.10$, and $x = 0.15$ are representative of the three phase fields α_{ss}, α'_{ss}, and β_{ss}, respectively.

The specimens quenched from 1200°C and slowly cooled to room temperature were essentially the same as those quenched from 1500°C except that the end member composition of the cubic$_{ss}$ phase, as indicated by the unit cell dimension, seemed to vary.

Hereafter we refer to the low-temperature form of $KAlO_2$ as α-$KAlO_2$, the high-temperature form as β-$KAlO_2$, and their respective solid solutions as α_{ss} and β_{ss}. The new phase that occurs at room temperature between about $x = 0.10$ and 0.125 is labeled α'_{ss}.

Trends in Unit Cell Dimensions

The unit cell dimensions for the 1500°C quenched specimens as a function of composition are presented in Table 1. As the XRD data show that these three phases clearly possess a common parent, namely, cristobalite-type with $a_p \approx 7.7$ Å, it is possible to observe the trends in the parent unit cell dimensions across the subject composition range by scaling the resultant dimensions appropriately. These normalized unit cell dimensions are plotted as a function of composition in Fig. 2.

For α_{ss} there is an overall increase in the unit cell dimensions with increasing silica content, whereas for α'_{ss} and β_{ss} there is an approximately linear decrease in dimension with composition to the end member composition for the β_{ss} phase in the $x = 0.25$ specimen. This allows an estimate of the end member composition as $x \approx 0.235$ for the β_{ss} phase quenched from 1500°C ($a = 7.7555(6)$ Å). For the 1200°C quench series the unit cell dimension for the end member was smaller at $a = 7.747(1)$ Å and smaller again for the specimen slowly cooled to room temperature at $a = 7.7368(7)$ Å, suggesting that either the composition range for β_{ss} is increased at lower temperatures or that the cubic unit cell dimension is somehow dependent on thermal

TABLE 1
Refined Unit Cell Dimensions

		Dimension (Å)		
Composition x	Phase	a	b	c
0.0	α_{ss}	5.4327(8)	10.924(2)	15.469(2)
0.025	α_{ss}	5.433(2)	10.931(4)	15.451(3)
0.5	α_{ss}	5.444(1)	10.938(3)	15.464(7)
0.075	α_{ss}	5.444(4)	10.901(9)	15.432(13)
0.1	α'_{ss}	21.767(2)		15.381(4)
0.125	α'_{ss}	21.735(3)		15.369(2)
0.15	β_{ss}	7.6799(7)		
0.175	β_{ss}	7.6750(6)		
0.2	β_{ss}	7.6659(7)		
0.25	β_{ss}	7.6555(6)		

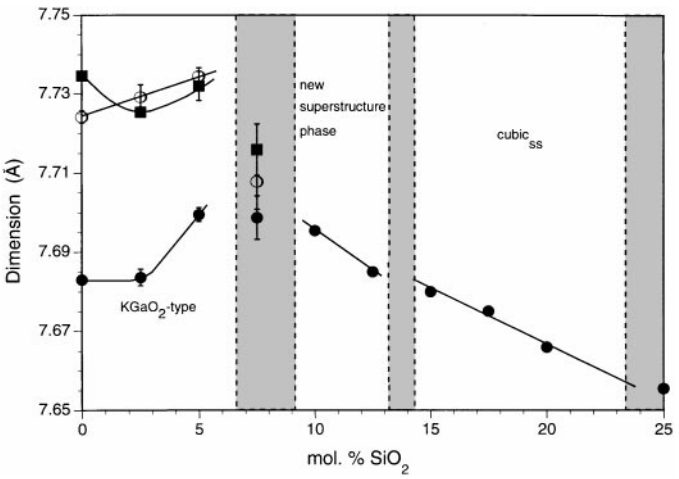

FIG. 2. Plot of the normalized refined unit cell dimensions for the system ($K_{1-x}Al_{1-x}Si_xO_2$, $0 \le x \le 0.25$). The data are normalized to their common parent, namely, *C*9 cristobalite-type with $a_p \approx 7.7$ Å, to facilitate comparison. For α_{ss}, $a_{norm} = \sqrt{2}a$ (●), $b_{norm} = 1/\sqrt{2}\, b$ (○), and $c_{norm} = \frac{1}{2}c$ (■); for α'_{ss}, $a_{norm} = c_{norm} = 1/\sqrt{8}\ a = \frac{1}{2}c$ (●); and for β_{ss}, $a_{norm} = a$ (●).

history. The unit cell dimensions for the 1200°C and slow-cooled samples at the other compositions ($x = 0.1$ and 0.2) indicated that there was at least some dependence of the room-temperature unit cell dimension on thermal history.

Determination of Unit Cell and Space Group of α-$KAlO_2$

Careful measurement of Guinier-Hägg films of the equilibrium specimens allowed us to index the XRD lines to an orthorhombic unit cell with dimensions $a = 5.4327(8)$, $b = 10.924(2)$, and $c = 15.469(2)$ Å, an ~0.7% distortion from a metrically cubic unit cell. The resolution of the orthorhombic line splitting was not observable if the specimen was insufficiently annealed or exposed to the atmosphere even for a few tens of seconds. These data agreed with the proposition of Pistorius and de Vries (12) that α-$KAlO_2$ was probably $KGaO_2$-type in that the observed unit cell dimensions and extinction conditions (15) were consistent with the $KGaO_2$-type space group symmetry *Pbca*. Further confirmation that α-$KAlO_2$ was indeed $KGaO_2$-type was obtained by calculating the XRD profile for this unit cell using the revised fractional coordinates for $KGaO_2$ listed in Grey *et al.* (16) and substituting Al atoms for Ga atoms in the calculation. The agreement between calculated and observed intensities was remarkably good. A complete listing of the indexed XRD data is given in Table 2.

Proposed Superstructure for the α'_{ss} Phase

The Guinier-Hägg films for specimens at $x = 0.10$ and $x = 0.125$ comprised a set of lines that could be indexed to a cubic unit cell with $Fd\bar{3}m$ symmetry and at least five additional lines. The lack of any splitting of the parent unit cell lines and the small number of additional lines initially caused us to be sceptical that we had identified a new phase. However, careful measurement of the additional lines showed an exact relationship between the parent and additional reflections. Unfortunately electron diffraction analysis of the subject materials using a transmission electron microscope, which we have used successfully in earlier studies of sodium aluminosilicates (7, 17) and sodium magnesiosilicates (18) to confirm unit cell dimensions and space group symmetry of cristobalite-related oxides, was not possible due to their reactivity in the atmosphere and susceptibility to electron beam damage.

The XRD data for the α'_{ss} phase could be indexed to a tetragonal superstructure of a cristobalite parent with $a_r = 2\sqrt{2}a_p$ and $c_r = 2c_p$. The refined unit cell dimensions for $x = 0.10$ were $a = 21.767(2)$ and $c = 15.381(4)$ Å. A complete listing of the indexed XRD data in terms of this tetragonal unit cell is given in Table 3. To allow a full comparison between the XRD data for α'_{ss} and β_{ss} we have

TABLE 2
α-$KAlO_2$ X-ray Powder Diffraction Data

h k l	I/I_0	d_{calc}	d_{obs}
0 2 2	5	4.462	4.458
0 2 3	1	3.749	3.742
1 2 3	5	3.086	3.087
1 1 4	5	3.027	3.029
1 2 4	100	2.729	2.730
2 0 0	48	2.716	2.716
1 3 3	12	2.609	2.610
2 1 1	4	2.599	2.599
2 0 2	5	2.563	2.559
2 1 2	1	2.495	2.497
1 2 5	11	2.412	2.412
1 3 4	7	2.383	2.383
1 0 6	27	2.329	2.330
2 2 2	14	2.320	2.321
0 4 4	9	2.231	2.231
2 0 4	1	2.223	2.223
2 3 0	4	2.177	2.178
2 3 2	1	2.096	2.095
0 4 5	2	2.047	2.047
1 5 1	4	2.010	2.011
0 0 8	14	1.934	1.934
0 4 7	2	1.718	1.717
1 6 4	44	1.576	1.577
1 2 9	22	1.570	1.570
2 1 8	2	1.559	1.559
1 6 5	3	1.507	1.507
3 3 4	1	1.495	1.496
2 4 8	15	1.365	1.365
4 0 0	2	1.358	1.358
1 2 12	12	1.222	1.222
4 4 0	12	1.216	1.217

TABLE 3
$K_{1-x}Al_{1-x}Si_xO_2$ ($x = 0.10$) X-Ray Powder Diffraction Data

$h\,k\,l$[a]	$G + q$	I/I_0	d_{calc}	d_{obs}
4 0 2	1 1 1	32	4.442	4.445
7 1 2	2 2 0 + $\frac{1}{4}(\bar{2}04)$	1	2.858	2.858
8 0 0	2 2 0	100	2.721	2.722
4 1 5	1 1 3 + $\frac{1}{8}(\bar{2}2\bar{4}$	9	2.658	2.658
1 1 6	0 0 2 + $\frac{1}{4}(024)$	5	2.529	2.530
4 0 6	3 1 1	33	2.319	2.319
8 0 4	2 2 2	21	2.221	2.221
6 0 6	1 1 3 + $\frac{1}{4}(220)$	3	2.094	2.093
5 5 6	0 2 2 + $\frac{1}{4}(024)$	2	1.970	1.969
8 8 0[b]	4 0 0	21	1.924	1.924
12 0 2	3 3 1	4	1.765	1.765
12 4 4	4 2 2	83	1.571	1.571
16 0 0	4 4 0	25	1.360	1.361
16 4 2	5 3 1	5	1.301	1.301
16 8 0	6 2 0	25	1.217	1.216

[a] As the resultant tetragonal unit cell is metrically cubic all reflections can be indexed in many different ways—only one indexation is given for each.
[b] Reflection position interpolated from film without Si internal standard due to overlap with Si line.

included the indexed data for $x = 0.15$ from within the β_{ss} field (Table 4).

Using a modulated structure description (see, for example, Refs. 18–22) of this cristobalite-type oxide phase it is informative to consider the additional reflections as satellite reflections of the underlying C9 parent structure. The satellite reflections can then be reindexed as $G_p \pm q$ where G_p is an allowed β-cristobalite-type parent structure reflection and q is a modulation wavevector. The XRD data for $x = 0.10$ are also indexed in this way in Table 3. From this we can see that the five readily observed satellite reflections (all shown in Fig. 1) can be indexed as first-order satellites of three different modulation wavevectors; $\frac{1}{4}\langle 420\rangle_p^*$, $\frac{1}{8}\langle 224\rangle_p^*$, and $\frac{1}{4}\langle 220\rangle_p^*$.

TABLE 4
$K_{1-x}Al_{1-x}Si_xO_2$ ($x = 0.15$) X-ray Powder Diffraction Data

$h\,k\,l$	I/I_0	d_{calc}	d_{obs}
1 1 1	28	4.434	4.432
2 2 0	100	2.715	2.717
3 1 1	18	2.316	2.316
2 2 2	18	2.217	2.216
4 0 0	12	1.920	1.919
3 3 1	3	1.762	1.762
4 2 2	43	1.568	1.568
4 4 0	14	1.358	1.357
5 3 1	3	1.298	1.298
6 2 0	14	1.214	1.214
4 4 4	22	1.109	1.107

It is interesting to note that the modulation wavevector $\frac{1}{4}\langle 220\rangle_p^*$ is very common among the cristobalite-type oxide derivative structures (see Refs. 19, 21–23), whereas $\frac{1}{4}\langle 420\rangle_p^*$ has only been observed once before, in the recently reported $2a_p$ cubic superstructure in the system $Na_{2-x}Al_{2-x}Si_xO_4$ at $x \approx 0.55$ (7, 21). The modulation wavevector $\frac{1}{8}\langle 224\rangle_p^*$ has no precedent. Without the satellite reflection at 33.65° 2θ the remaining four reflections could be indexed to a smaller $2a_p$ cubic superstructure. Nevertheless the reflection at 33.65° 2θ is real and the strongest of the satellite reflections and requires the adoption of the $2\sqrt{2}a_p \times 2c_p$ unit cell.

While it is highly speculative, the $\frac{1}{8}\langle 224\rangle_p^*$ modulation that requires this large supercell may be indirectly associated with the composition of the α'_{ss} phase that occurs at or close to 12.5 mol% SiO_2; i.e., one-eighth of the tetrahedral framework sites are occupied by Si. What is more certain is that the modulation of the underlying cristobalite-type structure is displacive in origin rather than compositional due to the absence of any low-angle ($< 30°$ 2θ) satellite reflections (cf. the modulated cristobalite-type sodium aluminosilicates reported in Ref. 18).

Structure Refinement of α-$KAlO_2$

The XRD profile of α-$KAlO_2$ for Rietveld refinement was extracted from Guinier-Hägg film ($\lambda = 1.5406$ Å), as described above. The program GSAS (23), which allows soft contraints on interatomic distances, was used for structure refinement.

The starting model was derived from the revised structure of $KGaO_2$ (16) with the framework cation site occupied by Al instead of Ga. With the atomic positions fixed at these starting positions the profile was refined using 21 variables: scale, profile (pseudo Voigt type 2—GW and LY), background (cosine Fourier series No. 2–12 coefficients), unit cell dimensions, and isotropic thermal parameters (like atoms constrained to be equal). The positional parameters were then refined with soft constraints on d_{Al-O} and d_{O-O} of 1.757 ± 0.01 and 2.869 ± 0.02 Å, respectively, to force the model to be chemically plausible. The final refinement statistics were $Rp = 0.049$, $wRp = 0.065$, and reduced $\chi^2 = 0.07$.

During preliminary refinement cycles it became evident that the parent $Fd\bar{3}m$ cristobalite-type reflections were on a significantly different scale than the satellite reflections; i.e., all the parent reflections were undercalculating and all the satellite reflections overcalculating. This was attributed to disorder and/or stacking faults in α-$KAlO_2$. Discussion of this phenomen in cristobalite-related oxides can be found in Section 11 of Ref. (22). For this reason the stronger parent reflections were excluded during profile refinement to minimize this scaling problem. The above scaling problem can not be attributed to preferred orientation.

The observed, calculated, and difference profiles for this model are shown in Fig. 3. The final refined atomic

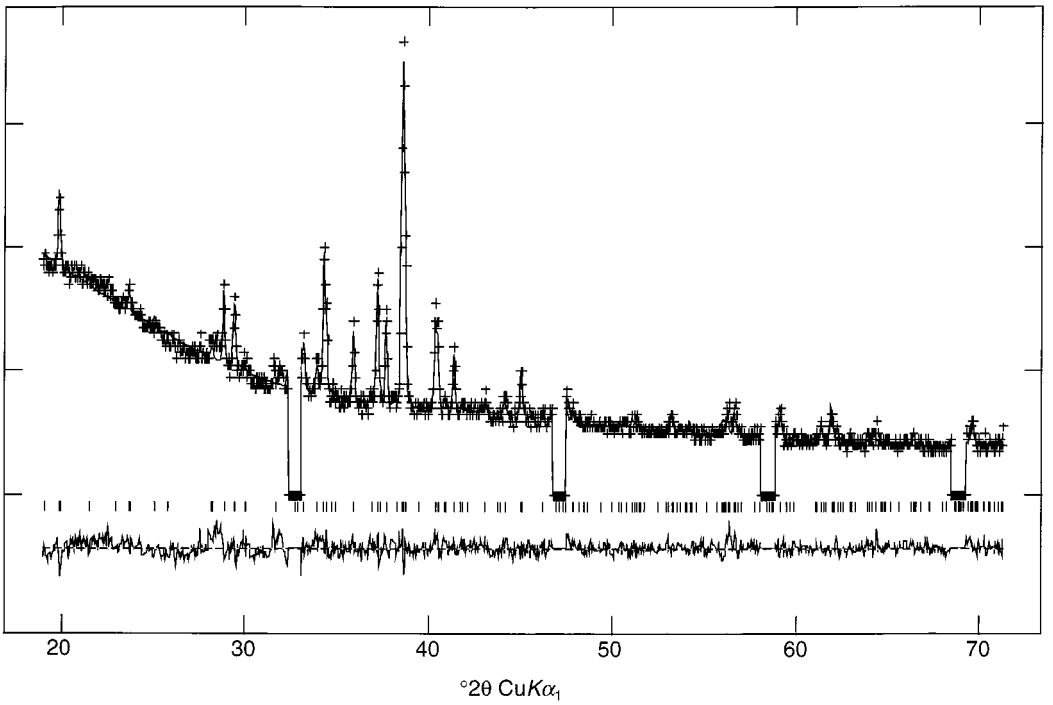

FIG. 3. Observed, calculated, and difference profiles from the Rietveld refinement of the XRD data for α-$KAlO_2$ between 19 and 72° 2θ. The observed data points are shown as + and the calculated profile is shown as a continuous line. The four excluded regions correspond to the strong parent reflections 220_p, 400_p, 422_p, and 440_p, respectively.

parameters, which are similar to those reported for $KGaO_2$ (16), and bond valence sums (24, 25) for atoms in the refined model are listed in Table 5.

Proposed Temperature-Composition Phase Diagram for $K_{1-x}Al_{1-x}Si_xO_2$, $0 \leq x \leq 0.25$

Reproducible thermodynamic events observed in the DSC data collected for 1500°C quenched specimens from $x = 0.0$ to 0.20 are summarized in Table 6. The two salient features are (i) the lowering of the $\beta_{ss} \leftrightarrow \alpha_{ss}$ phase transition with progressive substitution of SiO_2 into $KAlO_2$ (ii) the observation of the $\beta_{ss} \leftrightarrow \alpha'_{ss}$ phase transition for the $x = 0.10$ specimen. The latter observation gives further weight to the XRD evidence for the existence of a new cristobalite-related phase field in the subject system with a previously unreported structure type.

Combining the DSC and XRD data allows us to propose a temperature vs composition equilibrium phase diagram (Fig. 4) for the system $K_{1-x}Al_{1-x}Si_xO_2$ for the K-rich region $0 \leq x \leq 0.25$. The detail provided in this phase diagram is fully consistent with and complementary to the equilibrium phase diagram for the $KAlO_2$–$KAlSiO_4$ join

TABLE 5
Refined Atomic Parameters for α-$KAlO_2$

Atom	x	y	z	$100 * U_{iso}$	Bond valence sum
Al1	0.259(1)	0.007(1)	0.188(1)	2.3(4)	3.03
Al2	0.280(1)	0.263(1)	0.063(1)	2.3(4)	3.00
K1	0.750(1)	0.009(1)	0.067(1)	3.8(3)	1.02
K2	0.795(1)	0.261(1)	0.190(1)	3.8(3)	0.87
O1	0.571(2)	0.286(1)	0.017(1)	2.9(6)	1.92
O2	0.170(1)	0.402(1)	0.107(1)	2.9(6)	2.06
O3	0.298(1)	0.155(1)	0.146(1)	2.9(6)	1.93
O4	0.046(1)	0.486(1)	0.278(1)	2.9(6)	2.01

TABLE 6
Differential Scanning Calorimetric Data for $K_{1-x}Al_{1-x}Si_xO_2$

	Heating		Cooling	
Composition x	Endotherm (°C)	Energy (Jg^{-1})	Exotherm (°C)	Energy (Jg^{-1})
0.0	541	10.2	531	10.8
0.025	440	5.4	430	6.9
0.050	332, 355	4.0	345, 323	3.5
0.075	—	—	—	—
0.10	224	2.5	229	3.0
0.125	—	—	—	—

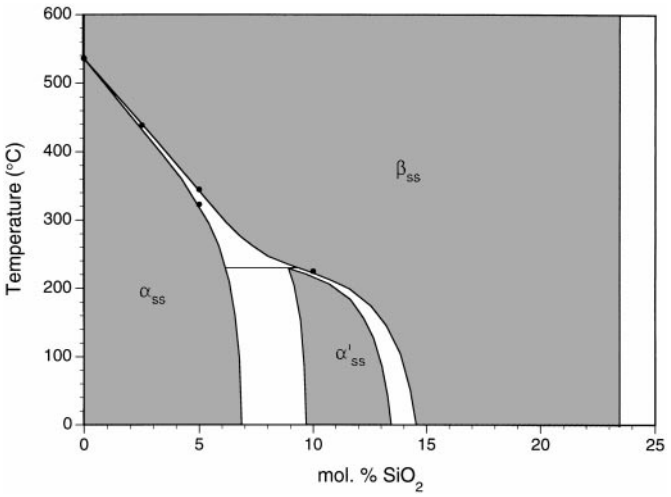

FIG. 4. Proposed temperature vs composition phase diagram from room temperature to 600°C for the K-rich end of the system $K_{1-x}Al_{1-x}Si_xO_2$ for $0 \leq x \leq 0.25$. Two phase fields are unshaded.

proposed by Roth (6). Confirmation of the proposed phase fields could be obtained by high-temperature XRD studies but, given the very high reactivity of the K-rich specimens with the atmosphere, achieving such data would be very challenging.

CONCLUSIONS

The equilibrium phase diagram proposed by Roth (6) for the $KAlO_2$–$KAlSi_2O_6$ binary join, which corresponds to $0 \leq x \leq 0.67$ in our formula $K_{1-x}Al_{1-x}Si_xO_2$, covers the temperature range 1300–2200°C. Our present results are in good agreement with those of Roth (6) in as much as they overlap. The new details provided by the present study all relate to temperatures well below 1300°C and are restricted to the cristobalite-related phases that all fall within the K-rich end of this binary join at $0 \leq x \leq 0.25$.

The low-temperature form of $KAlO_2$, α-$KAlO_2$, has the $KGaO_2$-type structure that is in accord with the suggestion of Pistorius and de Vries (12) in their study of $KFeO_2$. α_{ss}, therefore, also has the room-temperature $KGaO_2$-type structure. The high-temperature form of $KAlO_2$, β-$KAlO_2$, presumably has the β-cristobalite-type $Fd\bar{3}m$ structure based on the observation at room temperature that the β_{ss} phase has this structure. The evidence that we have presented in this study does point to the existence of a new cristobalite-related phase that we have called α'_{ss} phase. Due to the rather subtle differences between this and β_{ss} it could easily have been overlooked in earlier studies.

ACKNOWLEDGMENTS

The authors thank Mr. Marek Schmidt of the Research School of Physical Sciences and Engineering, ANU, for assistance with preliminary DTA measurements; Mr. Gordon Lockhart, of the Research School of Chemistry, ANU, for assistance in collecting the DSC data; Dr. Yasunori Tabira of the Research School of Chemistry, ANU, for digitizing the Guinier-Hägg films; and Dr. Ray Withers of the Research School of Chemistry, ANU, for helpful discussions.

REFERENCES

1. E. M. Levin, C. R. Robbins, and H. F. McMurdie, "Phase Diagrams for Ceramists," Vol. 1. (M. K. Reser, Ed.). The American Ceramic Society, Columbus, OH, 1964.
2. J. F. Schiarer and N. L. Bowen, *Am. J. Sci.* **253,** 681–746 (1955).
3. A.Yamaguchi, *Yogyo Kyokaishi* **78,** 74–75 (1970).
4. C. Li, A. F. Reid, and S. Saunders, *J. Solid State Chem.* **3,** 614 (1971).
5. L. P. Cook, R. S. Roth, H. S. Parker, and T. Negas, *Am. Mineral.* **62,** 1180–1190 (1977).
6. R. S. Roth, *Adv. Chem. Ser.* **186,** 391–408 (1980).
7. J. G. Thompson, A. Melnitchenko, S. R. Palethorpe, and R. L. Withers, *J. Solid State Chem.* **131,** 24 (1997).
8. L. T. Brownmiller, *Am. J. Sci.* **29,** 260 (1935).
9. T. F. W. Barth, *J. Chem. Phys.* **3,** 323–325 (1935).
10. Y. Otsubo, K. Yamaguchi, and Y. Kawamura, *Nippon Kagaku Zasshi* **83,** 352–353 (1962).
11. O. I. Arakelyan, *Khim. Prakt. Primen. Silik.* 63–71 (1960).
12. C. W. F. T. Pistorius and G. F. de Vries, *Z. Anorg. Allg. Chem.* **395,** 119 (1973).
13. E. T. Allen and H. F. Rogers, *Am. Chem. J.* **24,** 304–318 (1900).
14. G. Johansson, *Acta Chem. Scand.* **20,** 505–515 (1966).
15. "International Tables for Crystallography," (T. Hahn, Ed.), Vol. A, 4th ed., Kluwer Academic, Dordrecht, 1995.
16. I. E. Grey, B. F. Hoskins, and I. C. Masden, *J. Solid State Chem.* **85,** 202 (1990).
17. J. G. Thompson, R. L. Withers, A. K.Whittaker, R. M. Traill, and J. D. Fitz Gerald, *J. Solid State Chem.* **104,** 59–73 (1993).
18. R. L. Withers, C. Lobo, J. G. Thompson, S. Schmid, and R. Stranger, *Acta Crystallogr. Sect. B* **53,** 203 (1997).
19. R. L. Withers and J. G. Thompson, *Acta Crystallogr. Sect. B* **49,** 614 (1993).
20. J. G. Thompson, R. L. Withers, A. Melnitchenko, and S. R. Palethorpe, *Acta Crystallogr. Sect. B* **54,** 531–546 (1998).
21. R. L. Withers, J. G. Thompson, A. Melnitchenko, and S. R. Palethorpe, *Acta Crystallogr. Sect. B* **54,** 547–557 (1998).
22. J. G. Thompson, R. L. Withers, S. R. Palethorpe, and A. Melnitchenko, *J. Solid State Chem.* **141,** 29–49 (1998).
23. A. C. Larson and R.B. von Dreele, "GSAS. The General Structure Analysis System." Los Alamos, NM, 1991.
24. I. D. Brown and D. Altermatt, *Acta Crystallogr. Sect. B* **41,** 244 (1985).
25. N. E. Brese and M. O'Keeffe, *Acta Crystallogr. Sect. B* **47,** 192 (1991).